# Plasmonic band structures in doped graphene tubes

Yu Zhou,[1,2] Ying-Ying Zhu,[1] Kun Zhang,[1] Hong-Wei Wu,[1] Ru-Wen Peng,[1,3] Ren-Hao Fan,[1] and Mu Wang[1,4]

[1]*National Laboratory of Solid State Microstructures, School of Physics, and Collaborative Innovation Center of Advanced Microstructures, Nanjing University, Nanjing 210093, China*
[2]*School of Science, Hangzhou Dianzi University, Hangzhou, 310018, China*
[3]*rwpeng@nju.edu.cn*
[4]*muwang@nju.edu.cn*

**Abstract:** We present theoretically the transport of plasmonic waves in doped graphene tube, which is made by rolling planar graphene sheet into a cylinder and periodic doping is applied on it. It is shown that periodic modulation of the Fermi level along the tube can open gaps in the dispersion relations of graphene plasmons and eventually create plasmonic band structures. The propagation of graphene plasmons is forbidden within the bandgaps; while within the band, the plasmonic waves present axially-extended field distributions and propagate along the tubes, yet well confined around the curved graphene surface. Furthermore, the bandgaps, propagation constants and propagation lengths of the modes in plasmonic band structures are significantly tuned by varying the Fermi level of graphene, which provides active controls over the plasmonic waves. Our proposed structures here may provide an approach to dynamically control the plasmonic waves in graphene-based subwavelength waveguides.

### References and links

1. A. K. Geim and K. S. Novoselov, "The rise of graphene," Nat. Mater. **6**(3), 183–191 (2007).
2. A. H. Castro Neto, F. Guinea, N. M. R. Peres, K. S. Novoselov, and A. K. Geim, "The electronic properties of graphene," Rev. Mod. Phys. **81**(1), 109–162 (2009).
3. F. H. L. Koppens, D. E. Chang, and F. J. García de Abajo, "Graphene plasmonics: a platform for strong light-matter interactions," Nano Lett. **11**(8), 3370–3377 (2011).
4. A. N. Grigorenko, M. Polini, and K. S. Novoselov, "Graphene plasmonics," Nat. Photonics **6**(11), 749–758 (2012).
5. Q. Bao and K. P. Loh, "Graphene photonics, plasmonics, and broadband optoelectronic devices," ACS Nano **6**(5), 3677–3694 (2012).
6. F. J. García de Abajo, "Graphene plasmonics: challenges and opportunities," ACS Photonics **1**(3), 135–152 (2014).
7. A. Yu. Nikitin, F. Guinea, F. J. Garcia-Vidal, and L. Martin-Moreno, "Fields radiated by a nanoemitter in a graphene sheet," Phys. Rev. B **84**(19), 195446 (2011).
8. T. R. Zhan, F. Y. Zhao, X. H. Hu, X. H. Liu, and J. Zi, Phys. Rev. B, "Band structure of plasmons and optical absorption enhancement in graphene on subwavelength dielectric gratings at infrared frequencies," **86**, 165416 (2012).
9. S. Thongrattanasiri, F. H. L. Koppens, and F. J. García de Abajo, "Complete optical absorption in periodically patterned graphene," Phys. Rev. Lett. **108**(4), 047401 (2012).
10. S. Thongrattanasiri and F. J. García de Abajo, "Optical field enhancement by strong plasmon interaction in graphene nanostructures," Phys. Rev. Lett. **110**(18), 187401 (2013).
11. Y. Zhou, Y. Q. Dong, R. H. Fan, Q. Hu, R. W. Peng, and M. Wang, "Asymmetric transmission of terahertz waves through a graphene-loaded metal grating," Appl. Phys. Lett. **105**(4), 041114 (2014).
12. Y. Zhou, C. Wang, D. H. Xu, R. H. Fan, K. Zhang, R. W. Peng, Q. Hu, and M. Wang, "Tuning the dispersion relation of a plasmonic waveguide via graphene contact," Europhys. Lett. **107**(3), 34007 (2014).
13. T. Stauber, G. Gómez-Santos, and F. J. García de Abajo, "Extraordinary absorption of decorated undoped graphene," Phys. Rev. Lett. **112**(7), 077401 (2014).
14. I. S. Lamata, P. Alonso-González, R. Hillenbrand, and A. Yu. Nikitin, "Plasmons in cylindrical 2D materials as a platform for nanophotonic circuits," ACS Photonics **2**(2), 280–286 (2015).

15. S. A. Mikhailov and K. Ziegler, "New electromagnetic mode in graphene," Phys. Rev. Lett. **99**(1), 016803 (2007).
16. M. Jablan, H. Buljan, and M. Soljačić, "Plasmonics in graphene at infrared frequencies," Phys. Rev. B **80**(24), 245435 (2009).
17. A. Yu. Nikitin, F. Guinea, F. J. García-Vidal, and L. Martín-Moreno, "Edge and waveguide terahertz surface plasmon modes in graphene microribbons," Phys. Rev. B **84**(16), 161407 (2011).
18. W. Wang, S. P. Apell, and J. M. Kinaret, "Edge magnetoplasmons and the optical excitations in graphene disks," Phys. Rev. B **86**(12), 125450 (2012).
19. J. Christensen, A. Manjavacas, S. Thongrattanasiri, F. H. L. Koppens, and F. J. García de Abajo, "Graphene plasmon waveguiding and hybridization in individual and paired nanoribbons," ACS Nano **6**(1), 431–440 (2012).
20. A. Croy, D. Midtvedt, A. Isacsson, and J. M. Kinaret, "Nonlinear damping in graphene resonators," Phys. Rev. B **86**(23), 235435 (2012).
21. S. Thongrattanasiri, I. Silveiro, and F. J. García de Abajo, "Plasmons in electrostatically doped graphene," Appl. Phys. Lett. **100**(20), 201105 (2012).
22. A. Yu. Nikitin, F. Guinea, F. J. Garcia-Vidal, and L. Martin-Moreno, "Surface plasmon enhanced absorption and suppressed transmission in periodic arrays of graphene ribbons," Phys. Rev. B **85**(8), 081405 (2012).
23. W. Wang and J. M. Kinaret, "Plasmons in graphene nanoribbons: Interband transitions and nonlocal effects," Phys. Rev. B **87**(19), 195424 (2013).
24. M. Gullans, D. E. Chang, F. H. L. Koppens, F. J. García de Abajo, and M. D. Lukin, "Single-photon nonlinear optics with graphene plasmons," Phys. Rev. Lett. **111**(24), 247401 (2013).
25. A. Yu. Nikitin, T. Low, and L. Martin-Moreno, "Anomalous reflection phase of graphene plasmons and its influence on resonators," Phys. Rev. B **90**(4), 041407 (2014).
26. T. Zhan, D. Han, X. Hu, X. Liu, S. T. Chui, and J. Zi, "Tunable terahertz radiation from graphene induced by moving electrons," Phys. Rev. B **89**(24), 245434 (2014).
27. Y. Gao, G. Ren, B. Zhu, H. Liu, Y. Lian, and S. Jian, "Analytical model for plasmon modes in graphene-coated nanowire," Opt. Express **22**(20), 24322–24331 (2014).
28. Y. Gao, G. Ren, B. Zhu, J. Wang, and S. Jian, "Single-mode graphene-coated nanowire plasmonic waveguide," Opt. Lett. **39**(20), 5909–5912 (2014).
29. R. J. Li, X. Lin, S. S. Lin, X. Liu, and H. S. Chen, "Tunable deep-subwavelength superscattering using graphene monolayers," Opt. Lett. **40**(8), 1651–1654 (2015).
30. T. H. Xiao, L. Gan, and Z. Y. Li, "Graphene surface plasmon polaritons transport on curved substrates," Photon. Res. **3**(6), 300–307 (2015).
31. T. J. Arruda, A. S. Martinez, and F. A. Pinheiro, "Omnidirectional absorption and off-resonance field enhancement in dielectric cylinders coated with graphene layers," J. Opt. Soc. Am. A **32**(5), 943–948 (2015).
32. D. A. Kuzmin, I. V. Bychkov, V. G. Shavrov, V. V. Temnov, H. I. Lee, and J. Mok, "Plasmonically induced magnetic field in graphene-coated nanowires," Opt. Lett. **41**(2), 396–399 (2016).
33. A. R. Davoyan and N. Engheta, "Salient features of deeply subwavelength guiding of terahertz radiation in graphene-coated fibers," ACS Photonics **3**(5), 737–742 (2016).
34. E. Yablonovitch, "Inhibited spontaneous emission in solid-state physics and electronics," Phys. Rev. Lett. **58**(20), 2059–2062 (1987).
35. Z. Wang, C. Y. Xia, S. Meloni, C. S. Zhou, and Y. Moreno, "Impact of social punishment on cooperative behavior in complex networks," Sci. Rep. **3**(1), 3055 (2013).
36. A. Vakil and N. Engheta, "Transformation optics using graphene," Science **332**(6035), 1291–1294 (2011).
37. H. J. Xu, W. B. Lu, W. Zhu, and Z. G. Dong, "Efficient manipulation of surface plasmon polariton waves in graphene," Appl. Phys. Lett. **100**(24), 243110 (2012).
38. Y. V. Bludov, N. M. R. Peres, and M. I. Vasilevskiy, "Graphene-based polaritonic crystal," Phys. Rev. B **85**(24), 245409 (2012).
39. T. Zhan, X. Shi, Y. Dai, X. Liu, and J. Zi, "Transfer matrix method for optics in graphene layers," J. Phys. Condens. Matter **25**(21), 215301 (2013).
40. H. W. Wu, F. Wang, Y. Q. Dong, F. Z. Shu, K. Zhang, R. W. Peng, X. Xiong, and M. Wang, "Cavity modes with optical orbital angular momentum in a metamaterial ring based on transformation optics," Opt. Express **23**(25), 32087–32097 (2015).
41. M. Jung, P. Rickhaus, S. Zihlmann, P. Makk, and C. Schönenberger, "Microwave photodetection in an ultraclean suspended bilayer graphene p-n junction," Nano Lett. **16**(11), 6988–6993 (2016).
42. N. Liu, H. Tian, G. Schwartz, J. B. H. Tok, T. L. Ren, and Z. Bao, "Large-area, transparent, and flexible infrared photodetector fabricated using P-N junctions formed by N-doping chemical vapor deposition grown graphene," Nano Lett. **14**(7), 3702–3708 (2014).
43. Z. Fang, Y. Wang, Z. Liu, A. Schlather, P. M. Ajayan, F. H. Koppens, P. Nordlander, and N. J. Halas, "Plasmon-induced doping of graphene," ACS Nano **6**(11), 10222–10228 (2012).

## 1. Introduction

Graphene is a gapless semiconductor constructed by arranging carbon atoms in a honeycomb lattice [1,2]. Recently, this atomic monolayer of carbon has been proven to be a promising

photonic and plasmonic material because it exhibits unprecedentedly strong light-matter interactions and tight electromagnetic field confinements [3–14]. For example, graphene sheets and ribbons have been proposed as plasmonic waveguides at infrared and terahertz frequencies [15–26]. The dispersion relation of graphene plasmons depends not only on the physical structure but also on the Fermi level, *i.e.*, they can be dynamically modified through-electrostatic gating, thereby providing a tunable platform for plasmonic applications. Very recently, graphene tubes, or similarly graphene-coated nanowires, have been theoretically proposed as single-mode plasmonic waveguides in the terahertz frequencies [27–33]. The dispersion relations of the plasmons in a uniformly doped graphene tube are continuous across certain frequency ranges: the fundamental mode has a dispersion curve that is continuous in the whole spectrum, and the high-order modes exhibit continuous dispersion curves above their cut-off frequencies [27,28]. Variation of the Fermi level of graphene merely adjusts the mode propagation constants, wave propagation can still happen in these systems. This means that uniformly doped graphene tubes have no selectivity over frequencies: the tube will let all the electromagnetic waves pass regardless of the frequency. However, especially in nanoelectric and nanophotonic applications, the emerging of energy bandgaps is the key to enable new functionalities. Such band gaps can be opened by coherent superposition of the reflected waves. Typical examples are photonic crystals, which were initially proposed to inhibit spontaneous emissions in atoms [34]. To create band gaps, periodic variation of the parameters is always required [35]. In the case of graphene tube, such variation can be achieved by periodic doping along the propagation direction; by doing this, plasmonic band structures may occur, which can be dynamically tuned by the Fermi level.

In this work, we propose a graphene tube with periodic variation of the Fermi level along the propagation direction. The dispersion relations of such tubes are found discontinuous, *i.e.*, bandgaps are opened. The plasmonic waves present standing-wave-like axial field distributions and propagate along the tubes only within the band, yet confined around curved graphene surface. Plasmonic bands with different azimuthal indexes are uncoupled, and cut-off frequencies exist for high-order modes. Taking advantage of the tunability of graphene, the bandgaps, the propagation constants and the propagation lengths of the plasmonic modes in such graphene tube can be significantly tuned by varying the Fermi level of those graphene building blocks, which provides active controls over plasmonic waves.

## 2. Plasmonic band structures in doped graphene tubes

We first consider the propagation of graphene plasmons in doped graphene tube, which is made by rolling planar graphene sheet into a cylinder and periodic doping is applied on it. It is known that plasmonic waves in graphene are supported by its in-plane conductivity. Here we use highly n-doped graphene tube to carry the plasmonic waves at low-frequency terahertz (THz) regime, thus only intraband transition is contributed to the graphene conductivity, which satisfies $\sigma(\omega) = ie^2 E_F / [\pi\hbar^2(\omega + i\tau^{-1})]$. $E_F$ is the Fermi level and $\tau$ is the relaxation time [36,37]. In calculations, the relaxation energy $E_\tau = 2\pi\hbar/\tau = 0.1$ meV is chosen for taking account of the losses. For simplicity, we assume that the curvature of the tube has no effects on the graphene conductivity, and the tube is in vacuum. Due to the fact that graphene is a one-atom-thick material, the boundary conditions used for deriving the plasmonic band structures are: (1) the tangential electric fields are continuous across the graphene layer, and (2) the discontinuity of the tangential magnetic fields equals the surface current density in graphene. These two boundary conditions have been widely used in the research of graphene plasmons [38,39]. In this work, we consider the case where the graphene tube consists of a series of building blocks, and each building block contains two sections with specific Fermi level $E_{Fi}$ ($i = 1, 2$) and length $P_i$ ($i = 1, 2$). The periodicity of the conductivity along the tube can be taken into account by adding its Fourier components: $\sigma(z) = \sum_n \sigma_n \exp(i2n\pi z/p)$,

where $p = P_1 + P_2$ denotes the period. $\sigma_n = [\int_{-p/2}^{p/2} dz\sigma(z)\exp(-i2n\pi z/p)]/p$ and $n$ is an integer. For this reason, the electromagnetic fields inside and outside the tube must be decomposed using the same Fourier bases. Thus, the $z$ components of the electric/magnetic fields can be written as:

$$E_z/H_z = \exp(ik_z z)\sum_n a_n \mathbf{B}_m(k_{r,n}r)\exp(i2\pi nz/p)\exp(im\theta). \qquad (1)$$

where $\mathbf{B}_m$ denotes the Bessel function. For inside and outside the tube, we respectively have $\mathbf{B}_m = \mathbf{I}_m$ and $\mathbf{B}_m = \mathbf{K}_m$, where $\mathbf{I}_m$ and $\mathbf{K}_m$ are respectively $m$-order modified Bessel functions of the first and second kind. $k_z$ is the propagation constant, $k_{r,n} = \sqrt{k_{z,n}^2 - k_0^2}$, $k_{z,n} = k_z + 2\pi n/p$, and $k_0$ is the wavenumber in vacuum. $a_n$ is a constant which describes the amplitude of the $n$-th order Fourier component, and $R$ is the radius of the tube. $m$ in $\exp(im\theta)$ is the azimuthal index, which in fact describes the orbital angular momentum of the plasmonic mode [40]. Other components of the fields can be derived from Eq. (1). The plasmonic band structures in the graphene tube are determined by the boundary conditions. For a certain azimuthal index $m$, a uniform graphene tube supports only one plasmonic mode under the light line [27,28]. This fact still holds under periodic doping conditions, since the periodicity is only along the tube which will not mix the plasmonic modes with different orbital angular momentums or azimuthal indexes. After tedious calculations, one can derive a determinant that contains infinite numbers of linear equations:

$$\begin{vmatrix} \mathbf{K}_m \delta_{n,n'} & \mathbf{0} & -\mathbf{I}_m \delta_{n,n'} & \mathbf{0} \\ \beta_n \mathbf{K}_m \delta_{n,n'} & \alpha_n k_r^n \mathbf{K}'_m \delta_{n,n'} & -\beta_n \mathbf{I}_m \delta_{n,n'} & -\alpha_n k_r^n \mathbf{I}'_m \delta_{n,n'} \\ -\alpha_n k_r^n \mathbf{K}'_m \delta_{n,n'} - \overline{\sigma}_{n-n'}\cdot \mathbf{K}_m & \beta_n \mathbf{K}_m \delta_{n,n'} & -\alpha_n k_r^n \mathbf{I}'_m \delta_{n,n'} - \overline{\sigma}_{n-n'}\cdot \mathbf{I}_m & -\beta_n \mathbf{I}_m \delta_{n,n'} \\ -\overline{\sigma}_{n-n'}\beta_{n'} \mathbf{K}_m & -\mathbf{K}_m - \overline{\sigma}_{n-n'}\alpha_{n'} k_r^{n'} \mathbf{K}'_m & -\overline{\sigma}_{n-n'}\beta_{n'} \mathbf{I}_m & \mathbf{I}_m - \overline{\sigma}_{n-n'}\cdot \alpha_{n'} k_r^{n'} \mathbf{I}'_m \end{vmatrix} = 0. \quad (2)$$

where $\alpha_n = -ik_0/(k_0^2 - k_{z,n}^2)$, $\beta_n = -mk_{zn}/R(k_0^2 - k_{zn}^2)$, $\overline{\sigma}_{n-n'} = \frac{1}{2}Z_0\sigma_{n-n'}$, $Z_0$ is the vacuum impedance, and $\delta_{n,n'}$ is Kronecker delta which is zero if $n = n'$. Here, $\mathbf{K}_m$ is short for $\mathbf{K}_m$ $(k_{r,n}R)$, and $\mathbf{I}_m$ is short for $\mathbf{I}_m(k_{r,n}R)$. Every element in Eq. (2) represents a $(2N + 1) \times (2N + 1)$ matrix, where N is the largest order of Fourier component we have considered. Actually in our following calculations, good accuracy can be achieved if we use more than 20 Fourier harmonics. Different Fourier components are coupled by the periodicity. The plasmonic band structure under specific azimuthal index can be derived by setting this determinant to zero.

Figure 1(a) shows the schematic of a uniform graphene tube. The propagation direction is along the $z$ axis, and the cross section of the tube is in the $x$-$y$ plane. The dispersion relation of the plasmonic mode with $m = 0$ is shown in Fig. 1(b); clearly, it is continuous across the whole spectrum. In the inset of Fig. 1(b), we show the transmission spectrum of THz waves propagating for the distance of 360 μm along the tube, which are calculated by using commercial software (FDTD Solutions, Lumerical). It is obvious that transmission is as high as 90% in a rather wide frequency range. The normalized $|E_z|^2$ at the point indicated by the black arrow in Fig. 1(b) is depicted in Fig. 1(c), which shows that the fields expand uniformly along the tube.

However, under periodic doping condition, situations are totally different. Figure 1(d) shows the schematic of a periodic graphene tube, where two different sections are respectively denoted with red and blue colors. The corresponding dispersion relation of this tube is plotted in Fig. 1(e); only half of the first Brillouin zone ($k_z > 0$) is presented. Due to the periodicity, the dispersion relation (black curve) is folded into the first Brillouin zone, causing multiple intersections with the light line (red line). At the edge and center of the

Brillouin zone, bandgaps are opened. In the gaps, the propagation of the plasmonic waves is forbidden. Besides, the inset of Fig. 1(e) shows the transmission spectrum of the THz waves propagating through 12 periods (total distance is 360μm along the tube) of such structure. The transmission drops below ~10% within the gap, while still remains approximately 90% outside the gap. The corresponding normalized $|E_z|^2$ at the point indicated by the black arrow in Fig. 1(e) is depicted in Fig. 1(f), showing periodic variation of the intensity along the tube. Actually in such a periodically doped graphene tube, periodic modulation provides additional reciprocal vector to compensate the momentum difference between the plasmons and free-space waves. As a consequence, the Bloch mode are excited by illuminating THz waves directly on the periodic structures. Thus, under periodic doping conditions, graphene tube indeed possesses plasmonic band structure, and the fields also exhibit periodicity in intensity during the propagation.
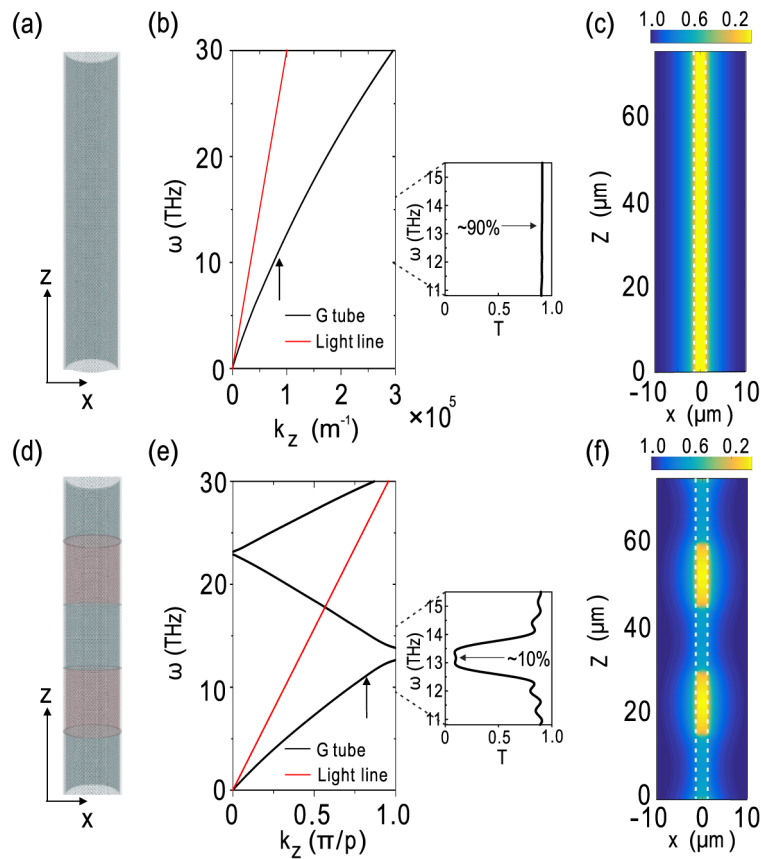


Fig. 1. (a) Schematic of a uniformly electron-doped graphene tube. (b) Dispersion relation of the uniform graphene tube (denoted as G tube), where $E_F = 0.6$ eV, and $R = 1$ μm. The inset shows the transmission spectrum of THz waves propagating for the 360μm-long distance along the tube. (c) The normalized $|E_z|^2$ at the point of the dispersion relation indicated by the black arrow in (b). The tube is indicated by white dashed lines. (d) Schematic of a periodically doped graphene tube. The two sections are denoted by different colors. (e) Band structure of the periodic graphene tube, where $P_1 = P_2 = 15$ μm, $R = 1$ μm, $E_{F1} = 0.7$ eV, $E_{F2} = 0.5$ eV, and the azimuthal index is zero ($m = 0$). The inset shows the transmission spectrum of THz waves propagating for 12 periods (the total distance is 360 μm) along the tube. (f) The normalized $|E_z|^2$ at the point of the band structure indicated by the black arrow in (e). The tube is denoted by white dashed lines.

Plasmonic band structures of the periodically doped graphene tubes can be classified according to the azimuthal index. Here we set the parameters of the tube as $P_1 = P_2 = 2$ μm, $R = 1$ μm, $E_{F1} = 0.7$ eV, and $E_{F2} = 0.5$ eV. For $m = 0$, the dispersion curve starts from zero frequency and exhibits gaps at the edge and center of the Brillouin zone, as shown by the black curves in Fig. 2(a). The dispersion relation of this plasmonic mode has multiple intersections with the light line (the red line in Fig. 2(a)). Under the light line, the electromagnetic fields are evanescent; thus, they are strictly confined near the tube and guided along the $z$ axis. However, above the light line, partial electromagnetic fields may be scattered into the far-field areas; the plasmonic waves would propagate along the tube, while simultaneously being scattered away. The normalized $|E_z|^2$ in the $x$-$z$ plane corresponding to the lower edge of the first band gap (indicated by the black arrow in Fig. 2(a)) is plotted in Fig. 2(d). At the edge of the band gap, the field intensity profile looks like a standing-wave, showing no sign of propagation. The normalized $|E_z|^2$ in the $x$-$y$ plane (see Fig. 2(g)) remains constant around the tube, corresponding to the case of $m = 0$.
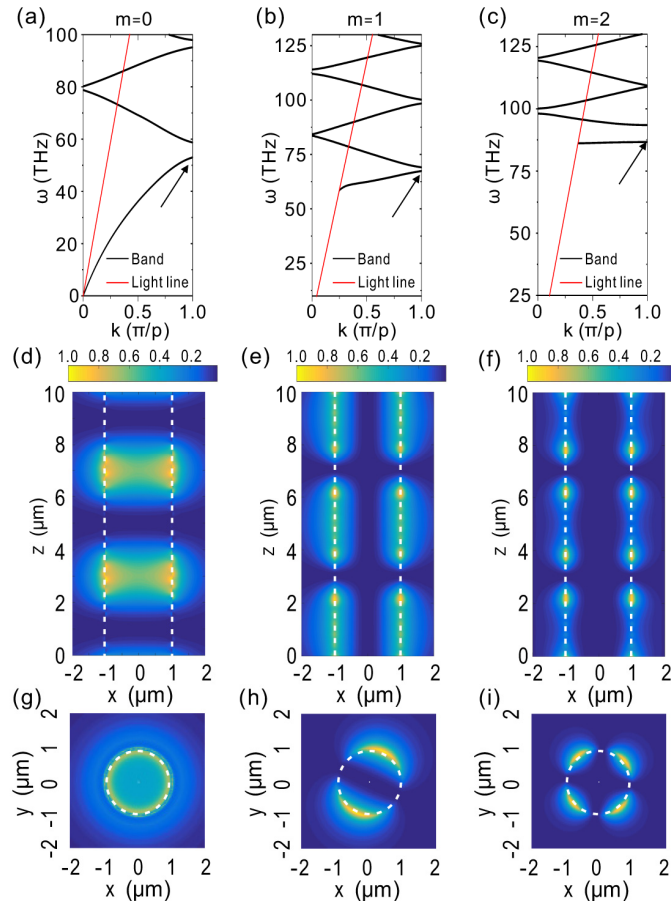


Fig. 2. Band structures of the periodically doped graphene tubes with (a) $m = 0$, (b) $m = 1$ and (c) $m = 2$. The parameters we chose are: $P_1 = P_2 = 2$ μm, $R = 1$ μm, $E_{F1} = 0.7$ eV, and $E_{F2} = 0.5$ eV. (d), (e) and (f) are the normalized $|E_z|^2$ at the $x$-$z$ plane at the edges of the first band gaps indicated by the black arrows in (a), (b) and (c), respectively. The tubes are indicated by white dashed lines. (g), (h) and (i) are the corresponding normalized $|E_z|^2$ at the $x$-$y$ plane, showing uniform, dipole-like and quadruple-like profiles around the tube, respectively.

The plasmonic band structure with $m = 1$ is plotted with black curves in Fig. 2(b). Compared with the case of $m = 0$, the dispersion relation has a cutoff frequency near $\omega = 53$ THz. The normalized $|E_z|^2$ in the $x$-$z$ plane corresponding to the lower edge of the first band gap (indicated by the black arrow in Fig. 2(b)) is shown in Fig. 2(e). Again, there is no sign of propagation. The fields are more tightly confined near the graphene layer. In the $x$-$y$ plane the normalized $|E_z|^2$ has a dipole-like profile around the tube (as shown in Fig. 2(h)), corresponding to the case of $m = 1$.

For the case of $m = 2$, the plasmonic dispersion also has a cut-off frequency near $\omega = 86$ THz, which is much higher than that of the $m = 1$ case. The field distribution in the $x$-$z$ plane corresponding to the lower edge of the first band gap (indicated by the black arrow in Fig. 2(c)) is depicted in Fig. 2(f). Also, the fields are extremely confined near the graphene layer and have standing wave-like intensity distributions along the $z$ axis. Due to the fact that $E_z$ has a factor of $\exp(im\theta)$, the profile of $|E_z|^2$ presents the dipole-like pattern for $m = 1$ (as shown in Fig. 2(h)) and a quadruple-like pattern for $m = 2$ (as shown in Fig. 2(i)). Despite their different azimuthal indexes, both dispersion relations exhibit bandgaps, within which no electromagnetic modes are found. The plasmonic waves within the bands can propagate along the tube with periodically varying field intensities. At the edge of the bandgaps, the plasmonic waves have standing wave-like profiles, indicating the stopping of tis propagation.

Selectively and individually gating graphene becomes a challenging problem if we concern real-world controllable fabrication. Fortunately, some techniques such as split gating method [41], patternable chemical doping [42], or even position-depend plamon-induced doping [43], have recently developed for nanofabrication. In our case, it is possible to use split gating method to achieve periodically-doped graphene tube, where electrical doping is applied individually by two sets of split gates. The doping levels of those two sets of building blocks are dependent of the gate pattern along the graphene tube. By changing the gate voltages individually, it is possible to realize a tunable doped graphene tube as we propose here.

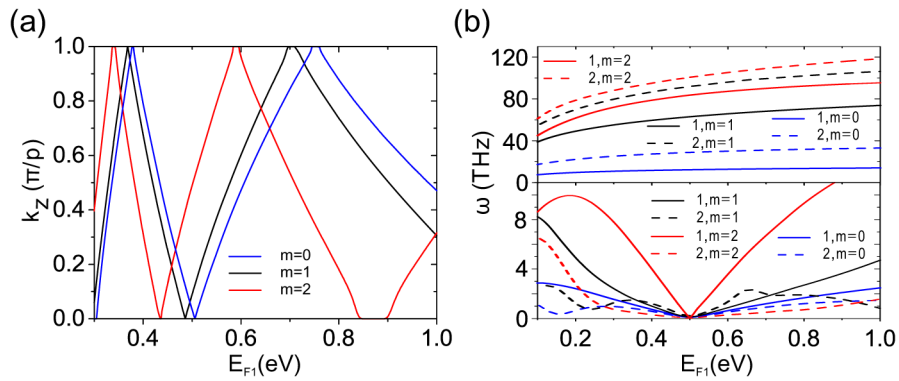## 3. Tunability of the plasmonic bandgaps and propagation lengths



Fig. 3. (a) $k_z$ of the plasmonic modes plotted as functions of $E_{F1}$. The frequency is fixed at 20 THz, $P_1 = P_2 = 2$ μm, $R = 1$ μm, and $E_{F2} = 0.5$ eV. Blue, black, and red curves respectively indicate $k_z$ of the modes with $m = 0$, $m = 1$ and $m = 2$. (b) The upper panel shows the central angular frequency $\omega$ of the band gaps as functions of $E_{F1}$. Only the first and the second gaps are plotted, denoted by the first number in the legends. Modes with $m = 0$, $m = 1$ and $m = 2$ are respectively denoted by blue, black, and red curves. The lower panel shows the corresponding widths of the band gaps as functions of $E_{F1}$. At $E_{F1} = 0.5$ eV, all gaps are closed.

The plasmonic band structures highly depend on the Fermi level and the length of each section in the building block. In the followings, we investigate the tunability of the bandgaps

and propagation lengths. For convenience, only the Fermi level of the first section ($E_{F1}$) is varied; other parameters are fixed. For a certain frequency (like in our case is 20 THz), the propagation constant $k_z$ depends on $E_{F1}$. Figure 3(a) shows the variations of the propagation constants of the plasmonic modes as $E_{F1}$ increases from 0.3 eV to 1 eV, while keeping $E_{F2}$ fixed at 0.5 eV. Other parameters are $P_1 = P_2 = 2$ μm, and $R = 1$ μm. Blue, black, and red curves denote the propagation constants for the $m = 0$, $m = 1$ and $m = 2$ modes, respectively. In some ranges, the propagation constants of the plasmonic modes reach the edge or center of the Brillouin zone, opening gaps in the dispersion curves. Modes with different azimuthal indexes show band gaps in different ranges of $E_{F1}$ ; thus, it is possible to selectively forbid the propagation of the plasmonic mode with a specific azimuthal index by carefully choosing the Fermi level. In Fig. 3(b), we show variations of the central frequencies (upper panel) and widths (lower panel) of the first and second band gaps as $E_{F1}$ increases from 0.1 eV to 1 eV. The solid and dashed curves in the upper panel respectively indicate the central frequencies for the first and second band gaps. Blue, black, and red colors denote the plasmonic modes with $m = 0$, $m = 1$ and $m = 2$, respectively. As we can see from the upper panel, the central frequencies gently increase as the Fermi level moves up. The variations of the widths of the band gaps are shown in the lower panel of Fig. 3(b). The first band gaps seem wider than the second ones for all cases. This may be caused by the absence of scattering near the first band gap, since it is completely under the light line. All gaps are closed when $E_{F1} = 0.5$ eV.

In real-world applications, propagation length is another important factor of plasmonic waveguides. In the case of periodically doped graphene tube, the scattering of electromagnetic waves into the far-field is completely inhibited under the light line. Thus, the remaining limitations are ohmic losses and plasmonic band gaps. We have investigated the propagation length of the plasmonic mode in Fig. 1(e). The propagation length (denoted as $L$, red curves) and the wavelength-normalized propagation length (denoted as $L/\lambda$, black curves) are plotted as functions of the frequency in Fig. 4(a). The wavelength becomes infinitely large in the low-frequency limit, while the propagation length is finite; thus, the wavelength-normalized propagation length must tend to zero as the frequency goes to zero. However, it can reach as large as 30 near $f = 1.8$ THz. More interestingly, the wavelength-normalized propagation length suddenly drops as the frequency further increases. This sudden drop is due to the fact that the corresponding frequency is approaching the first band gap.
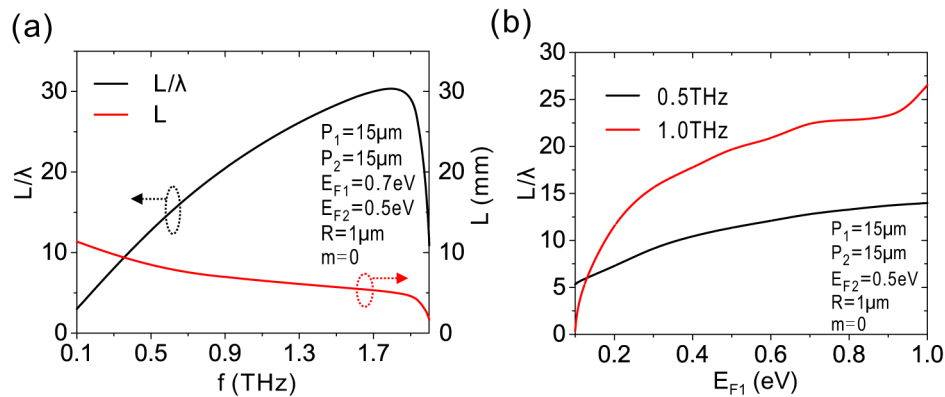


Fig. 4. (a) The propagation length, $L$, and wavelength normalized propagation length, $L/\lambda$, of the plasmonic mode under the first band gap in Fig. 1(e) as functions of the frequency. The remaining parameters are $P_1 = P_2 = 15$ μm, $R = 1$ μm, $E_{F1} = 0.7$ eV, $E_{F2} = 0.5$ eV, and $m = 0$. (b) Normalized propagation lengths as functions of $E_{F1}$ at two different frequencies. Other parameters are denoted therein.

The propagation length also depends on the Fermi level as we expected. Similarly, we investigate variations of the normalized propagation lengths at two frequencies as $E_{F1}$ is

increased from 0.1 eV to 1 eV, while other parameters are fixed, see Fig. 4(b). For 1 THz (red curve in Fig. 4(b)), the propagation length tends to zero as $E_{F1}$ approaches 0.1 eV. This is due to the fact that the frequency of 1 THz in this case is very close to the band gap. When $E_{F1} =$ 1.0 eV, the propagation length of the 1 THz plasmonic wave can reach over 25 times the excitation wavelength. For 0.5 THz (black curve in Fig. 4(b)), since the band gap is far away from this frequency in such range of $E_{F1}$, the propagation length of the plasmonic wave varies gently due to the ohmic loss of graphene.

## 4. Conclusions

In this work, we have proposed a doped graphene tube and demonstrated that periodic doping along a graphene tube can create plasmonic band structures. Within the bandgaps, the propagation of plasmonic waves is prohibited; while within the band, the plasmonic waves propagate along the tubes, yet confined around curved graphene surface. For the plasmonic modes with nonzero azimuthal index, cutoff frequency exists and the electromagnetic fields are extremely confined around the tube. The bandgaps, propagation constants and propagation lengths of the modes in plasmonic band structures can be significantly tuned by varying the Fermi level of graphene, which makes it possible to active control the propagation of plasmonic waves. The investigations may provide a way to dynamically engineer plasmonic band structures and efficiently control the plasmonic waves in graphene-based subwavelength waveguides.